

Article

Detailed Power Loss Analysis of T-Type Neutral Point Clamped Converter for Reactive Power Compensation

Marcin Zygmanski 

Power Electronics, Electrical Drives and Robotics Department, Faculty of Electrical Engineering, Silesian University of Technology, 44-100 Gliwice, Poland; marcin.zygmanski@polsl.pl

Abstract: The paper presents an analysis of power losses in a three-phase T-type neutral point clamped converter with insulated gate bipolar transistors. The paper's main aim is to perform a detailed analysis of power losses in the converter operating as an active power filter. The study is based on the use of characteristics of semiconductor devices provided by the manufacturer in the module datasheet. Thanks to the analysis, it is possible to recognise the value of power losses, which facilitates the design of the converter cooling system. Identifying how power losses are distributed between the module switching devices is also possible. Power losses are shown as functions of the output current and module temperature. The analysis results were successfully verified by measuring power losses using a laboratory model of the converter with rated currents of 10 and 20 A. The obtained results indicate relatively low power losses and a relatively even distribution of power losses between the semiconductor devices. This is a superior feature of the three-level T-type neutral point clamped converter topology.

Keywords: power losses; three-level T-type neutral point converter; active power filter operation



Citation: Zygmanski, M. Detailed Power Loss Analysis of T-Type Neutral Point Clamped Converter for Reactive Power Compensation. *Electronics* **2022**, *11*, 2129. <https://doi.org/10.3390/electronics11142129>

Academic Editor: Juan Rodríguez Méndez

Received: 23 June 2022

Accepted: 6 July 2022

Published: 7 July 2022

Publisher's Note: MDPI stays neutral with regard to jurisdictional claims in published maps and institutional affiliations.



Copyright: © 2022 by the author. Licensee MDPI, Basel, Switzerland. This article is an open access article distributed under the terms and conditions of the Creative Commons Attribution (CC BY) license (<https://creativecommons.org/licenses/by/4.0/>).

1. Introduction

1.1. Motivations

Power losses in power electronic converters play a crucial role in the design of their cooling system. Better recognition of power losses allows the converter designers to choose the appropriate cooling system in terms of its performance and size. This paper presents a detailed analysis of the power losses of the T-type Neutral Point Clamped (TNPC) converter, which is applied to the active power filter. The selection of this converter topology is dictated by the relatively low power losses and the fact that in this topology, as in other three-level topologies, the middle point of the dc circuit is available. In the case of an active filter, the neutral wire is connected to this middle point so that a fourth converter leg is not required. An additional advantage of the selected converter, in relation to the classical two-level topology, is the possibility of reducing the dimensions and the cost of the grid-side passive filter.

1.2. Literature Review

The topologies of multilevel converters were developed more than twenty years ago [1,2]. Multilevel converters were introduced mainly because of their possible use in converting medium voltage energy. Thanks to these converters, it was possible to efficiently convert electrical energy without using expensive and large transformers [3,4]. Over the years, it has become clear that many multilevel converter topologies often have better performance parameters than the classic two-level converter, even at low voltage levels [5–9]. One of the most important features of these converters is high efficiency, which was not always an obvious fact with the greater number of semiconductor devices used in converters with a very high number of voltage levels [10–12]. The high efficiency of

the converter is an essential parameter because due to low power losses, the converter's lifetime is longer, and the total cost of its operation is lower [13].

Because power loss evaluation of converters is a complex and multivariable issue [14–19], it is crucial to identify power losses in converters operating under various conditions accurately. The knowledge about converter power losses is vital for designers of converter cooling systems and manufacturers of semiconductor modules. Nowadays, semiconductor modules can be optimised for one converter operating mode but will not be suitable for other operating conditions. For example, the module optimised for grid-tied PWM rectifiers has diodes with higher current ratings than the module optimised for the PWM inverter. Typically, power loss analysis is performed individually for each converter topology.

This paper analyses the three-phase T-type neutral point clamped (TNPC) converter. The converter belongs to the group of three-level converters [20] in which there are also classical neutral point clamped (NPC) converter [21], active neutral point clamped (ANPC) converter [22], and advanced neutral point clamped converter [23].

The NPC converter, apart from lower power losses and better output voltage waveform, is characterised by an uneven distribution of power losses among semiconductor devices [24]. The solution to this issue is the development of the ANPC converter, which, using transistors instead of clamping diodes, makes it possible to distribute power losses between the semiconductor devices better. A further improvement of the three-level converter is the TNPC converter [25]. The power losses of this converter are analysed in this article. A very advantageous feature of this converter is the lower number of semiconductor switches compared to the ANPC or NPC topologies and lower power losses [26].

The selection of the T-type neutral point clamped converter for the active power filter is made mainly based on the requirements for reducing the size of the grid filter and the dimensions of the cooling system. The second aspect, which directly relates to the power loss analysis, is a topic of this paper. The other reason for the selection of the 3-level topology is the access to the medium point of the dc-link circuit. By the connection of the neutral wire to the medium point, it is possible to reduce the number of necessary converter legs, which additionally reduces the converter losses.

The proposed method of calculating power losses in the TNPC converter is similar to the method proposed in [26]. The difference is that in [26–28], the semiconductor switch output characteristics have been approximated by linear functions. Still, in this paper, the approximation is made with more precise power functions that also recognise the influence of temperature on these characteristics. Further, the functions of energy losses are more accurately presented than in [26–28]. The results of power loss analysis are shown in this paper mainly as a function of the output current and temperature with the switching frequency and phase-shift angle set to constant values.

Currently, intensive works are ongoing worldwide on converters with SiC MOSFETs, such as the TNPC converter [29] or the ANPC hybrid converter combining the IGBTs with the SiC-MOSFETs in a single topology [30]. This topology is characterised by even lower power losses than the TNPC topology. Despite the increasing share of converters with SiC-MOSFET transistors, the topology of the TNPC converter using IGBT transistors still has good properties. Such properties include low power losses, favourable output voltage, and a low level of generated disturbances. It is believed that accurate recognition of the power loss is needed.

1.3. Contribution

The analysis presented in this paper is performed for the TNPC converter operating as an active filter. The details on the laboratory model of the TNPC converter are given in [31]. This converter practically generates reactive current with only a small share of power losses constituting the active power. Connecting the converter to the electrical grid causes the modulation index and the phase-shift angle to be almost constant. This, in turn, means that the analysis presented in the article can be performed with a limited number of changing parameters affecting power losses.

Power losses generated in the TNPC converter should be small due to the long operation time of the converter and the need for its long lifetime. In many cases, the lifetime of power electronic converters is approx. 20 years, during which even minor losses contribute to high costs for the end-user of the converter.

Many works on power losses in the TNPC converters are devoted to inverters with a phase-shift angle close to zero. For this mode of operation, the natural parameter is the converter efficiency, which, in the case of the converter operating as an active filter, cannot be used. The converter efficiency parameter is replaced in this paper by a per kVA power loss ratio. Such a parameter can be useful when comparing different converter topologies or different active filter solutions.

The main contributions of this paper are listed below.

- The development of a detailed analysis of power losses for the TNPC converter. This analysis allows the user to quickly determine the power losses when one or more operating parameters of the converter or its design parameters are changed. The developed power loss model of the TNPC converter is an analytical model that has an advantage over the simulation model because obtaining results in the form of characteristics is much faster. However, this is done at the expense of the use of a number of mathematical equations, which in the case of simulation models do not need to be used.
- The model uses an accurate approximation of characteristics of semiconductor devices for currents changed between 0 and the rated current value. This approximation guarantees that power losses are better mapped than in the case of using a model with a piecewise-linear approximation.
- The analysis proposed in the paper is based on characteristics obtained from the semiconductor datasheet. The development of such an analysis is faster when compared to analyses requiring the prior measurements in specific test circuits as is typically used in the literature, e.g., [27,28]. Using the datasheet characteristics can be done, however, when the parameters of the converter gate circuit and the dc-link circuit are comparable to the parameters used in the datasheet.
- The analysis proposed in the paper has regard to eight different parameters influencing the power losses they are (1) output current amplitude of the fundamental component, (2) dc-link voltage, (3) switching frequency, (4) phase-shift angle of the fundamental components of output current and voltage, (5) semiconductor temperature, (6) modulation index, (7) PWM modulation technique, and (8) gate resistances in a transistor driver circuit. Such analysis is comprehensive and can be applied to converters operating under different conditions. In this paper, the operational conditions are restricted to the operation of the active power filter.

It is believed that a detailed power loss analysis for the TNPC converter is needed and is an original contribution. In many papers, power losses are presented only for a specific case of converter operation, and this is mainly for the inverter operation. In this paper, power losses are shown more broadly.

1.4. Paper Organisation

This paper is organised as follows. Section 2 shows the complete power loss analysis in the TNPC converter. Section 3 presents the experimental validation of power loss analysis on the example of two test setups with TNPC converters. Section 4 presents the conclusions. After the conclusions, the nomenclature is presented in which all parameters used in this paper are listed. After that, Appendix A lists all values of the design parameters of the TNPC converter in the study.

2. Power Loss Analysis

Most converter power losses in power electronic converters are generated due to the conduction and switching of semiconductor devices. This paper only considers these two sources of losses generated in a T-type NPC converter without considering the dead-time

effect and dc-link voltage ripple. Both conduction and switching losses are calculated analytically based on approximated IGBT module characteristics provided by the manufacturer [32]. Although a single leg of the TNPC converter consists of four transistors and two diodes, as seen in Figure 1, power losses in only three semiconductor devices are considered. They are transistors T_1 and T_2 and diode D_4 . This approach is adopted because transistors T_1 and T_4 have the same parameters and are exposed to the same currents and voltages phase-shifted by half of the fundamental period. A similar situation exists for transistors T_2 and T_3 and diodes D_1 and D_4 . Other losses generated in the converter are also considered, among which are the dc-link capacitor losses and losses generated in pcb tracks due to resistance.

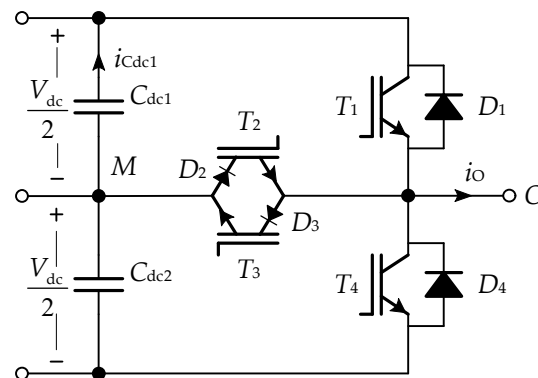


Figure 1. Single leg of the TNPC converter consisting of two conventional IGBTs, T_1 and T_4 , two reverse blocking RB-IGBTs, T_2 and T_3 , and two diodes, D_1 and D_4 .

2.1. Conduction Power Losses

The conduction losses (Equation (1)) are calculated separately for each switching device by calculating the average value of the power obtained from the integral of instantaneous power $p_X(t) = i_X(t) v_X(t)$, where $i_X(t)$ is the device X current and $v_X(t)$ is the voltage across this device. The integration of instantaneous power is performed in the ωt domain from angle α_1 to α_2 . Because the device current $i_X(\omega t)$ is a modulated phase current $i_O(\omega t)$, it must be multiplied by the modulation function $S_X(t)$, $i_X(\omega t) = i_O(\omega t) S_X(\omega t)$. The modulation function is closely related to the modulating signal $S_M(\omega t)$ used in the converter PWM modulator.

$$P_{conX}(T_X) = \frac{1}{2\pi} \int_{\alpha_1}^{\alpha_2} \{i_X(\omega t) \cdot v_X(\omega t, T_X)\} d\omega t = \frac{1}{2\pi} \int_{\alpha_1}^{\alpha_2} \{i_O(\omega t) \cdot S_X(\omega t) \cdot v_X(\omega t, T_X)\} d\omega t, \quad (1)$$

2.1.1. Output Characteristic Approximation

In the presented power loss analysis, the output current is assumed as sinusoidal, $i_O = I_m \sin(\omega t - \varphi)$, and the device voltage $v_X(t, T_X)$ is a function of the current and device junction temperature T_X as in Equation (2).

$$v_X(\omega t, T_X) = v_X(i_X(\omega t), T_X) = V_{X0}(T_X) + (V_{Xn}(T_X) - V_{X0}(T_X)) \left(\frac{i_X(\omega t)}{I_n} \right)^{\frac{1}{n_X(T_X)}}, \quad (2)$$

where $V_{X0}(T_X)$ is a temperature-varying threshold voltage, $V_{Xn}(T_X)$ is a temperature-varying device voltage at nominal current I_n , and $1/n_X(T_X)$ is a temperature-varying exponent of the power function representation of the device on-state characteristic. The threshold voltage $V_{X0}(T_X)$ and nominal voltage $V_{Xn}(T_X)$ are linear functions obtained from on-state characteristics at temperatures $T_X = 25$ and $T_X = 125$ °C (Equations (3) and (4)).

$$V_{X0}(T_X) = a_{X0}T_X + b_{X0} = \frac{V_{X0,125} - V_{X0,25}}{125\text{ }^\circ\text{C} - 25\text{ }^\circ\text{C}} T_X + V_{X0,25} - \frac{V_{X0,125} - V_{X0,25}}{125\text{ }^\circ\text{C} - 25\text{ }^\circ\text{C}} 25\text{ }^\circ\text{C}, \quad (3)$$

$$V_{Xn}(T_X) = a_{Xn}T_X + b_{Xn} = \frac{V_{Xn,125} - V_{Xn,25}}{125\text{ }^\circ\text{C} - 25\text{ }^\circ\text{C}}T_X + V_{Xn,25} - \frac{V_{Xn,125} - V_{Xn,25}}{125\text{ }^\circ\text{C} - 25\text{ }^\circ\text{C}}25\text{ }^\circ\text{C}, \quad (4)$$

The values of function parameters given in Equations (3) and (4) for the analysed IGBT TNPC module are listed in Table 1 and shown in Figure 2.

Table 1. Parameters of temperature-varying functions $V_{X0}(T_X)$ and nominal voltage $V_{Xn}(T_X)$ of transistors T_1 and T_2 and diode D_4 .

Device X	$V_{X0,25}$, V	$V_{X0,125}$, V	$V_{Xn,25}$, V	$V_{Xn,125}$, V	a_{X0} , V/°C	b_{X0} , V	a_{Xn} , V/°C	b_{Xn} , V
T_1	0.70	0.50	1.72	1.94	−0.002	0.750	0.0022	1.665
T_2	0.70	0.50	2.35	2.46	−0.002	0.750	0.0011	2.323
D_4	0.75	0.55	1.69	1.85	−0.002	0.800	0.0016	1.650

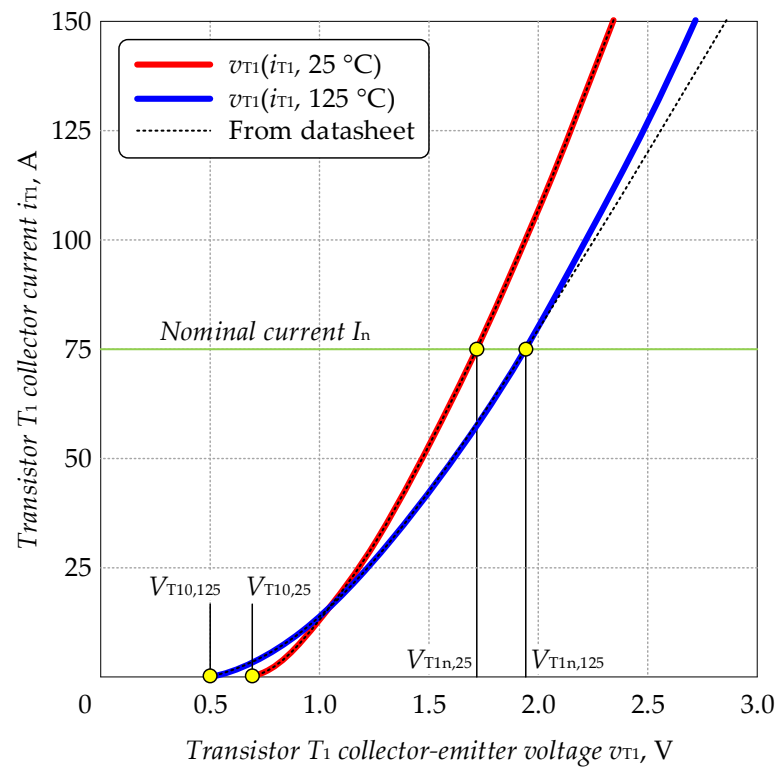


Figure 2. Output characteristic of transistor T_1 from the three-phase TNPC IGBT module 12MBI75VN120–50 ($V_{CES} = 1200\text{ V}$, $I_n = 75\text{ A}$).

Finding exponent $n_X(T_X)$ of the power function is performed by applying the curve fitting method to a normalised function (Equation (5)), which is obtained from Equation (2)

$$\frac{i_X}{I_n} = f(T_X) = \left(\frac{v_X(i_X, T_X) - V_{X0}(T_X)}{(V_{Xn}(T_X) - V_{X0}(T_X))} \right)^{n_X(T_X)}, \quad (5)$$

where $v_X(i_X, T_X)$ is the output characteristic voltage taken from the IGBT module datasheet. For transistor T_1 , the normalised function (Equation (5)) for $T_{T1} = 125\text{ }^\circ\text{C}$ is depicted in Figure 3. The normalised function (Equation (5)) always crosses points (0, 0) and (1, 1) even though the temperature T_X varies.

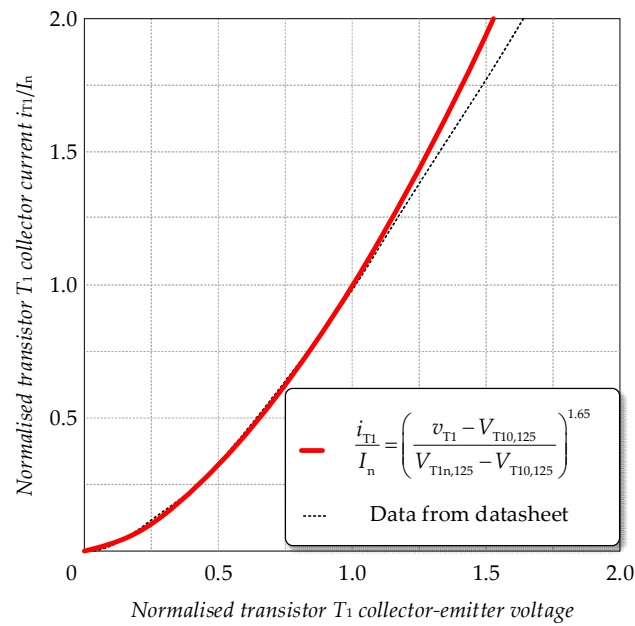


Figure 3. Normalised output characteristic of transistor T_1 from the TNPC module 12MBI75VN120-50 ($V_{CES} = 1200$ V, $I_n = 75$ A) for temperature $T_{T1} = 125$ °C.

In Figure 3, one can see that the normalised function i_{T1}/I_n for $T_{T1} = 125$ °C with $n_{T1}(125$ °C) = 1.65 matches the data for a normalised voltage in the range between 0 and 1. Still, for voltages between 1 and 2, some discrepancy is observed. This discrepancy is not problematic because it occurs for currents higher than the rated value I_n in the range, which is out of the scope of the analysis presented in this paper. The best-fitting exponents for normalised functions of all converter devices are collected in Table 2; these parameters are given for temperatures $T_X = 25$ and $T_X = 125$ °C.

Table 2. Exponents of power functions for output characteristics of all TNPC converter devices T_1 and T_2 and D_4 for two temperatures $T_X = 25$ and $T_X = 125$ °C.

Device X	$n_X(25$ °C)	$n_X(125$ °C)
T_1	1.51	1.65
T_2	1.71	1.66
D_4	1.89	1.81

The exponent $n_X(T_X)$ given in Equation (5) is a function of temperature T_X and is approximated by a linear function obtained from two points, $n_X(25$ °C) and $n_X(125$ °C), which are calculated from Equation (6).

$$n_X(T_X) = an_X T_X + bn_X = \frac{n_X(125 \text{ °C}) - n_X(25 \text{ °C})}{125 \text{ °C} - 25 \text{ °C}} T_X + n_X(25 \text{ °C}) - \frac{n_X(125 \text{ °C}) - n_X(25 \text{ °C})}{125 \text{ °C} - 25 \text{ °C}} 25 \text{ °C}, \quad (6)$$

After substituting Equations (2)–(6) into Equation (1), each device’s conduction losses are given as Equation (7).

$$P_{conX}(T_X) = \frac{1}{2\pi} \int_{\alpha_1}^{\alpha_2} \left\{ I_m \sin(\omega t - \varphi) \cdot S_X(t) \cdot \left[V_{X0}(T_X) + (V_{Xn}(T_X) - V_{X0}(T_X)) \left(\frac{I_m \sin(\omega t - \varphi)}{I_n} \right)^{\frac{1}{n_X(T_X)}} \right] \right\} d\omega t, \quad (7)$$

2.1.2. Conduction Angles and Modulation Function

Power loss analysis is performed in the ωt domain. Therefore, it is essential to identify the corresponding conduction angles for each semiconductor device in the TNPC converter

(Figure 1). All devices' currents for exemplary output current and modulation index m_a are shown in Figure 4.

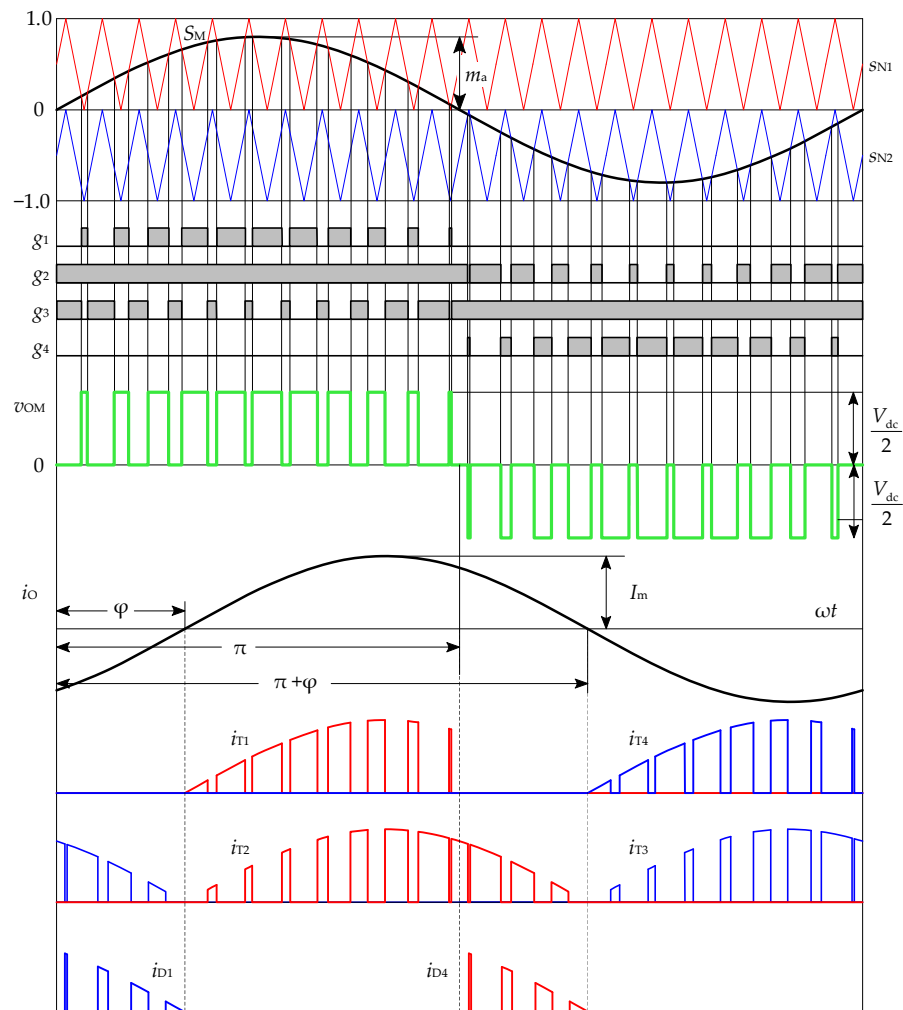


Figure 4. Output voltage v_{OM} and all device currents of TNPC single-leg for modulation index $m_a = 0.8$. (The switching frequency is intentionally reduced to improve the readability of the waveforms).

Each TNPC converter device conducts switched currents for different angles. The angle at which a device starts conducting is referred to as α_1 , and the angle when a device stops conducting the current is α_2 . Both angles are different for each converter device, as is seen in Figure 4 and Table 3. In Figure 4, device currents are modulated according to modulation functions $S_X(\omega t)$. For example, transistor T_1 's current, i_{T1} , is modulated by function $S_{T1}(\omega t) = S_M(\omega t)$, but transistor T_2 's current is modulated by the complementary function $S_{T2}(\omega t) = 1 - S_M(\omega t)$ for $\omega t = (0, \pi)$ and $S_{T2}(\omega t) = 1 + S_M(\omega t)$ for $\omega t = (\pi, 2\pi)$. Modulation functions of all device currents are given in Table 3.

Table 3. Conduction angles α_1 and α_2 and modulated functions $S_X(\omega t)$ of devices T_1, T_2 and D_1 .

Device X	α_1	α_2	$S_X(\omega t)$
T_1	φ	π	$S_M(\omega t)$
T_2	φ	$\pi + \varphi$	$1 - S_M(\omega t) $
D_4	π	$\pi + \varphi$	$-S_M(\omega t)$

2.1.3. Results of Conduction Power Losses

After substituting all parameters related to device output characteristics, conduction angles and modulation function into Equation (7), the total conduction power losses can be calculated. It is assumed that the output current is sinusoidal with the phase-shift-angle equal to $\varphi = \pi/2$ and the modulation index $m_a = 0.86$. The phase-shift angle $\varphi = \pi/2$ corresponds to the converter operation as a reactive power compensator. In practice, the converter operates with a small share of power losses, which reduces the phase-shift angle to nearly $\varphi = 89^\circ$. Since such a difference in the angles does not significantly impact the value of the power losses, the value of $\varphi = \pi/2$ is assumed. The analysis also assumes that power losses are calculated for the same junction temperature of all switching devices. The conduction losses of the three-phase TNPC converter given as a function of temperature T_j are depicted in Figure 5a. These losses are calculated as the sum of losses in all devices multiplied by the number of phases and duplicated due to the number of devices in each converter leg, $P_{\text{con}} = 6P_{\text{conT1}} + 6P_{\text{conT2}} + 6P_{\text{conD4}}$.

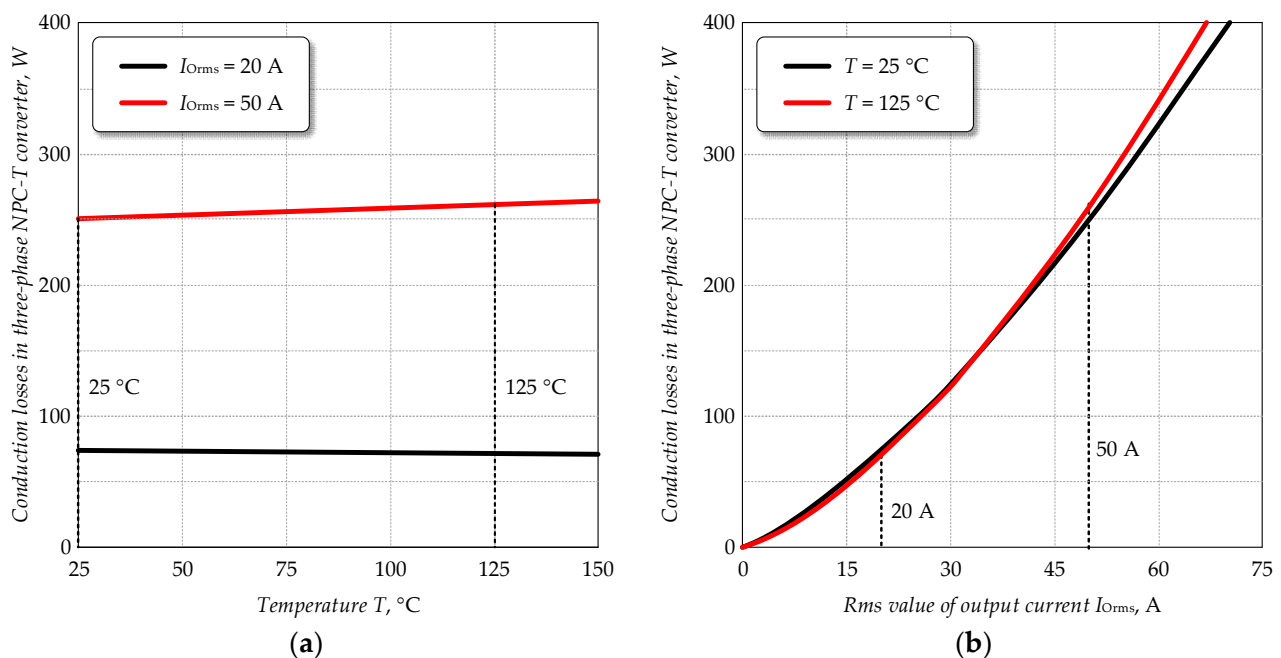


Figure 5. Conduction power losses of the three-phase TNPC converter for the modulation index $m_a = 0.86$ and the phase-shift angle $\varphi = \pi/2$ given as (a) a function of temperature for the output current rms value $I_{\text{Orms}} = 20$ and 50 A and (b) a function of the rms value of the output current for temperatures of 25 and 125 °C.

From the characteristics shown in Figure 5b, conduction power losses for the current of $I_{\text{Orms}} = 20$ A decrease with temperature increase. Such behaviour of power losses can be explained by the negative thermal coefficient occurring in output device characteristics present for currents below 15 A for transistors T_1 and T_4 (as in Figure 2), below 35 A for transistors T_2 and T_3 , and below 30 A for diodes D_1 and D_4 .

Conduction power losses for the device temperature of 25 °C and the output currents of $I_{\text{Orms}} = 20$ and 50 A equal 73.6 and 250.1 W, respectively. The distribution of conduction power losses among converter devices is not even, as presented in Figure 6.

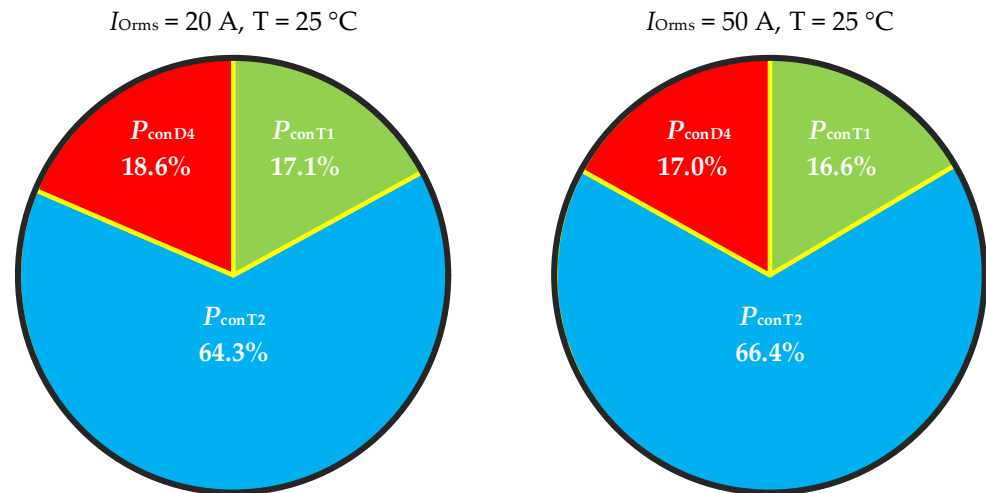


Figure 6. Distribution of conduction power losses among TNPC converter devices for modulation index $m_a = 0.86$ and the phase-shift angle $\varphi = \pi/2$, temperature $T = 25\text{ }^\circ\text{C}$ and two rms values of the output current 20 and 50 A.

From Figure 6, one can see that the distribution of conduction power losses for a constant phase-shift angle φ and modulation index m_a is slightly different with the change of the output current rms value. The RB-IGBT transistors T_2 and T_3 have the largest share of conduction losses. This is because these transistors conduct modulated currents for half of the fundamental period ($\alpha_2 - \alpha_1 = \pi$) compared to transistors T_1 and T_4 , which conduct modulated currents for $\alpha_2 - \alpha_1 = \pi - \varphi = \pi/2$ (for $\varphi = \pi/2$) and diodes D_1 and D_4 , which conduct such currents for $\alpha_2 - \alpha_1 = \pi + \varphi - \pi = \pi/2$.

2.2. Switching Power Losses

The TNPC converter has smaller switching power losses compared to other converters. This is because switching losses in transistors T_1 and T_4 occur at blocking voltages $V_{dc}/2$ even these transistors must withstand the entire V_{dc} similarly as in a two-level converter. In a two-level converter, power losses occur at voltages V_{dc} ; thus, switching losses, which are proportional to the blocking voltage, in the TNPC converter is reduced to half of such losses of a two-level converter. This is true when a TNPC converter uses identical transistors as a two-level converter. However, RB-IGBTs (T_2 and T_3) have better switching performance because they are designed for withstanding the voltage of $V_{dc}/2$.

Switching power losses are generated in IGBTs during transistor turn-on and turn-off processes. They can be calculated as an average value of a sum of energies during turn-on E_{on} and during turn-off E_{off} over the fundamental period multiplied by the switching frequency f_s . These energies are functions of the device current $i_X(\omega t)$, device temperature T_X , blocking voltage V_b and the resistances of the gate circuit R_G . In the presented analysis, resistances R_G are chosen to the same values selected by the manufacturer in the module datasheet [32]. However, due to the resistance of driver output, the resistances are equal $R_{G1} = 3.2\ \Omega$, $R_{G2} = 5.7\ \Omega$. The switching power losses are an integral of energies in the interval restricted by switching angles α_3 and α_4 (Equation (8)).

$$P_{swX}(T_X) = f_s \frac{1}{2\pi} \int_{\alpha_3}^{\alpha_4} \{E_{onX}(i_X(\omega t), T_X, V_b) + E_{offX}(i_X(\omega t), T_X, V_b) + E_{rrX}(i_X(\omega t), T_X, V_b)\} d\omega t, \quad (8)$$

where E_{rr} is the switching energy generated in the diode due to reverse recovery. For diodes, energies E_{on} and E_{off} are equal to zero; similarly, for transistors, E_{rr} is equal to zero.

2.2.1. Switching Angles

The switching angles α_3 and α_4 , which are not the same as conduction angles, can be shown by device current and voltage waveforms in Figure 7 and are listed in Table 4.

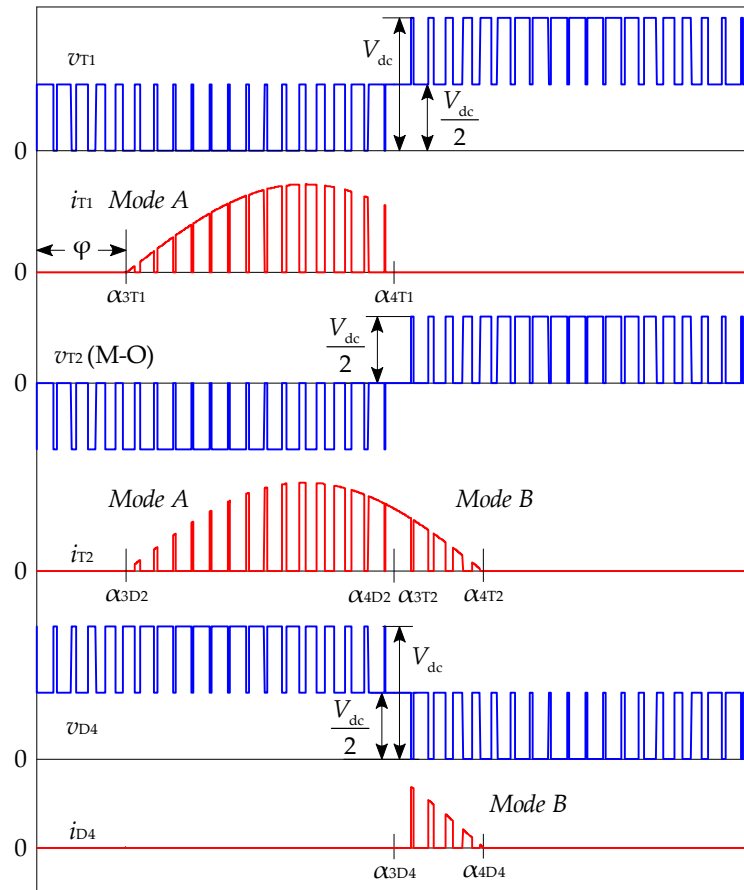


Figure 7. Current and voltage waveforms of devices T_1 , T_2 , D_2 and D_4 with marked switching angles α_3 and α_4 .

Table 4. Switching angles α_3 and α_4 of devices T_1 , T_2 , D_2 and D_4 with indicated switching mode.

Device X	α_3	α_4	Mode
T_1	φ	π	A
T_2	π	$\pi + \varphi$	B
D_2	φ	π	A
D_4	π	$\pi + \varphi$	B

Contrary to conduction losses, the switching losses in transistor T_2 and diode D_2 are calculated separately. The RB-IGBT conduction losses are taken together for transistor T_2 and diode D_2 , which are connected in series and are represented by a single output characteristic. The switching losses in RB-IGBT are separated for transistor T_2 and diode D_2 . For $0 < \omega t \leq \pi$, transistor T_2 is still turned on; thus, for positive device currents, which is for $\varphi < \omega t \leq \pi$, the switching power losses occur on diode D_2 due to its reverse recovery E_{rr} . This phenomenon can be explained by the fact that in this angle range, the voltage v_{T2} is switched between negative voltage $-V_{dc}/2$ and 0. For $i_{T2} > 0$ and $\pi < \omega t \leq \pi + \varphi$, switching losses are generated in transistor T_2 . In Table 4, one can see the modes of commutation (Mode A and Mode B), which correspond to modes distinguished by the manufacturer of the IGBT module. For Mode A, losses are generated in transistors T_1 and T_4 , but because the switching losses in T_4 are the same as in T_1 , only losses in T_1 are

calculated. In mode A, switching energies E_{rr} are generated in diodes D_2 and D_3 . In mode B, switching energies are generated in transistors T_2 (and T_3) and diodes D_4 and D_1 .

2.2.2. Characteristics of Switching Energies

All characteristics of switching energies E_{on} , E_{off} and E_{rr} are presented in Figure 8 as functions of the device current for both switching modes. These functions are given for two temperatures $T_X = 25$ and $T_X = 125$ °C, the blocking voltage $V_{dcref} = 300$ V, the gate resistors $R_{G1} = R_{G4} = 2.2$ Ω and $R_{G2} = R_{G3} = 4.7$ Ω and for the gate voltages ranging from -15 to $+15$ V.

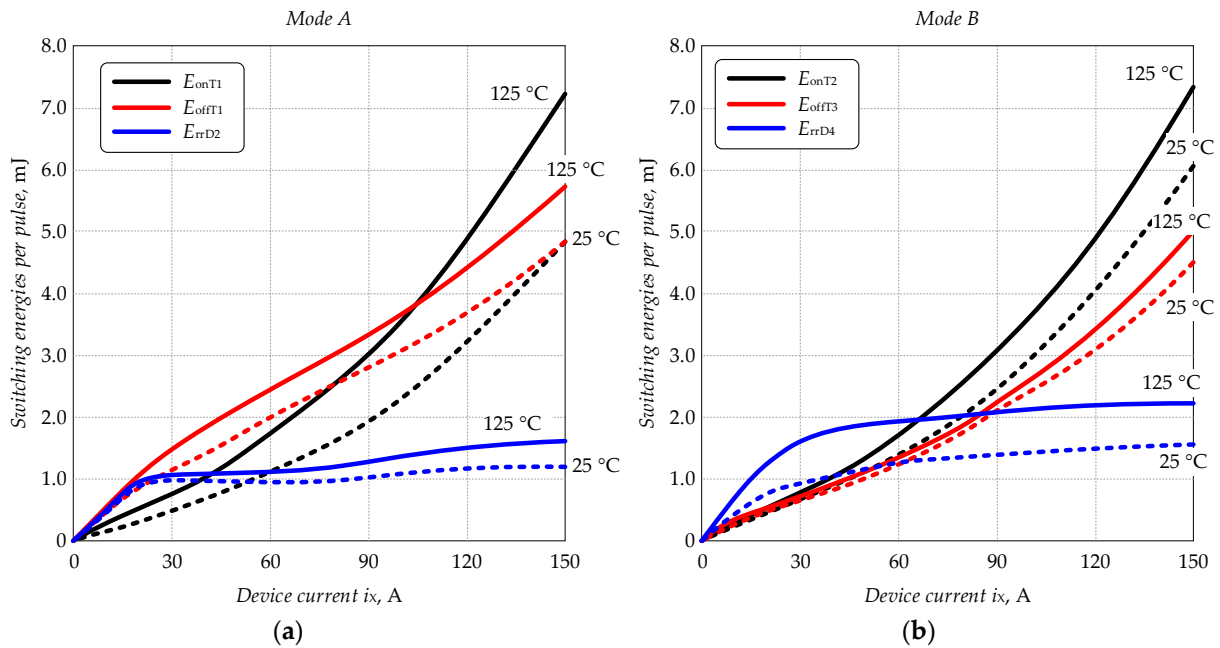


Figure 8. Switching energies given as a function of device current for module 12MBI75VN120-50, (a) in mode A, energies E_{on} and E_{off} occur in transistors T_1 and T_4 , reverse recovery energy E_{rr} occur in diodes D_2 and D_3 , (b) in mode B, energies E_{on} and E_{off} occur in transistors T_2 and T_3 , reverse recovery energy E_{rr} occur in diodes D_1 and D_4 .

Switching energy characteristics for transistors given in Figure 8 can be approximated by quadratic functions as in Equation (9) and multiplied by a factor k_{RGXY} representing the effect of the gate resistance on switching losses. The approximating function coefficients for device current from 0 to 75 A are listed in Table 5.

$$E_{YX,TX}(i_X) = k_{RGYX} \left(a_{YX,TX} i_X^2 + b_{YX,TX} i_X + c_{YX,TX} \right) \text{ for } Y = \{\text{on, off}\}, \quad (9)$$

Table 5. Coefficients of approximating quadratic functions of transistor switching energies as in Equation (9).

Device X	Switching Y	k_{RGYX}	T_X	$a_{YX} \times 10^{-9}, \text{J/A}^2$	$b_{YX} \times 10^{-6}, \text{J/A}$	$c_{YX} \times 10^{-6}, \text{J}$
T_1	on	1.083	25 °C	75.0	14.3	10.0
	on		125 °C	150.6	19.1	32.9
	off	1.010	25 °C	-107.1	39.2	44.2
	off		125 °C	-244.0	55.5	18.3
T_2	on	1.055	25 °C	47.6	20.4	18.3
	on		125 °C	95.2	22.5	38.3
	off	1.020	25 °C	45.8	17.6	21.3
	off		125 °C	-25.6	23.2	42.1

The approximation of diode reverse recovery energy characteristics by quadratic functions does not provide satisfactory results; therefore, the cubic function (Equation (10)) is chosen for these characteristics. The coefficients a_{YX} , b_{YX} , c_{YX} and d_{YX} are obtained using a fitting algorithm for device currents from 0 to 75 A.

$$E_{rrX,TX}(i_X) = k_{RGYX} \left(a_{rrX,TX} i_X^3 + b_{rrX,TX} i_X^2 + c_{rrX,TX} i_X + d_{rrX,TX} \right), \quad (10)$$

The approximating cubic function coefficients for reverse recovery energy losses in diodes are listed in Table 6.

Table 6. Coefficients of approximating cubic functions of diode reverse recovery energies.

Device X	T_X	k_{RGX}	$a_{rrX} \times 10^{-9}, \text{J/A}^3$	$b_{rrX} \times 10^{-6}, \text{J/A}^2$	$c_{rrX} \times 10^{-6}, \text{J/A}$	$d_{rrX} \times 10^{-6}, \text{J}$
D_2	25 °C	0.96	5.38	−0.88	54.1	−9.39
	125 °C		6.31	−1.25	85.3	−22.12
D_4	25 °C	1.00	8.84	−1.34	64.3	−10.30
	125 °C		9.32	−1.39	68.5	−0.76

The temperature influence on switching energies in each device is considered by approximation of each polynomial coefficient $z = a, b, c$ and d by linear function obtained from two points $z_{YX,25}$ (for $T_X = 25$ °C) and $z_{YX,125}$ (for $T_X = 125$ °C), which is given in Equation (11).

$$z_{YX}(T_X) = \frac{z_{YX,125} - z_{YX,25}}{125 \text{ °C} - 25 \text{ °C}} T_X + z_{YX,25} - \frac{z_{YX,125} - z_{YX,25}}{125 \text{ °C} - 25 \text{ °C}} 25 \text{ °C} \quad (11)$$

2.2.3. Results of Switching Power Losses

The calculation of switching power losses in all four semiconductor devices is performed using Equations (12)–(15). In the analysis, it is assumed that the junction temperature of all switching devices is the same, the switching frequency is $f_S = 20$ kHz, and the blocking voltage V_b is equal to $V_{dc}/2 = 370$ V (while the blocking voltage for which datasheet data is obtained is equal to $V_{dcref} = 300$ V). Total switching power losses in the three-phase TNPC converter is the sum of switching losses of all devices multiplied by six as in Equation (16).

$$P_{swT1}(T_{T1}) = f_S \frac{1}{2\pi} \frac{V_{dc}/2}{V_{dcref}} \int_{\varphi}^{\pi} \{E_{onT1}(i_{T1}(\omega t), T_{T1}) + E_{offT1}(i_{T1}(\omega t), T_{T1})\} d\omega t, \quad (12)$$

$$P_{swT2}(T_{T2}) = f_S \frac{1}{2\pi} \frac{V_{dc}/2}{V_{dcref}} \int_{\pi}^{\pi+\varphi} \{E_{onT2}(i_{T2}(\omega t), T_{T2}) + E_{offT2}(i_{T2}(\omega t), T_{T2})\} d\omega t, \quad (13)$$

$$P_{swD2}(T_{D2}) = f_S \frac{1}{2\pi} \frac{V_{dc}/2}{V_{dcref}} \int_{\varphi}^{\pi} \{E_{rrD2}(i_{D2}(\omega t), T_{D2})\} d\omega t, \quad (14)$$

$$P_{swD4}(T_{D4}) = f_S \frac{1}{2\pi} \frac{V_{dc}/2}{V_{dcref}} \int_{\pi}^{\pi+\varphi} \{E_{rrD4}(i_{D4}(\omega t), T_{D4})\} d\omega t, \quad (15)$$

$$P_{sw}(T) = 6(P_{swT1}(T) + P_{swT2}(T) + P_{swD2}(T) + P_{swD4}(T)), \quad (16)$$

The characteristic of switching power losses Equation (16), as a function of device temperature (with the assumption that all devices are exposed to the same temperature), is shown in Figure 9a. As presented, the switching losses increase with the temperature increase and are between 1.6 and 2.3 times higher than the conduction losses for $I_{Orms} = 20$ A and constitute 0.9 to 1.2 of conduction losses for $I_{Orms} = 50$ A. Unlike conduction power losses, switching losses (Equation (16)) always have a positive thermal coefficient, as shown in

Figure 9b. The switching power losses are nearly linear functions of current compared to quadratic functions for conduction losses.

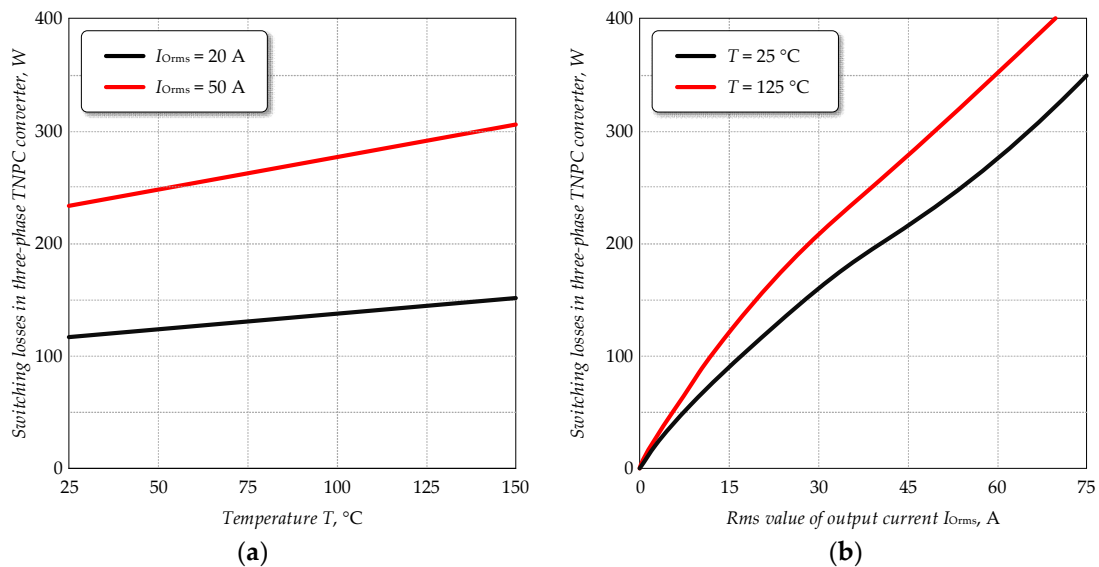


Figure 9. Switching power losses P_{sw} of three-phase TNPC converter for the switching frequency $f_S = 20$ kHz, half of dc-link voltage $V_{dc}/2 = 370$ V and the phase-shift angle $\varphi = \pi/2$ given as (a) a function of temperature for the output current rms value $I_{Orms} = 20$ and 50 A and (b) a function of the rms value of the output current for temperatures of 25 and 125 °C.

It is interesting that for small currents, switching losses converge to zero. This is because the output current is assumed as sinusoidal in the presented analysis. In the real converter, current ripples are present in the output current, increasing the switching losses particularly close to zero current fundamental components. This phenomenon is presented in the next section.

The distribution of switching losses among devices (Equations (12)–(15)) is presented in Figure 10 for the rms value of the output current $I_{Orms} = 20$ and $I_{Orms} = 50$ A. This distribution shows that the highest power losses occur in transistors T_1 and T_4 , opposite to the conduction losses where the highest losses occur in transistors T_2 and T_3 .

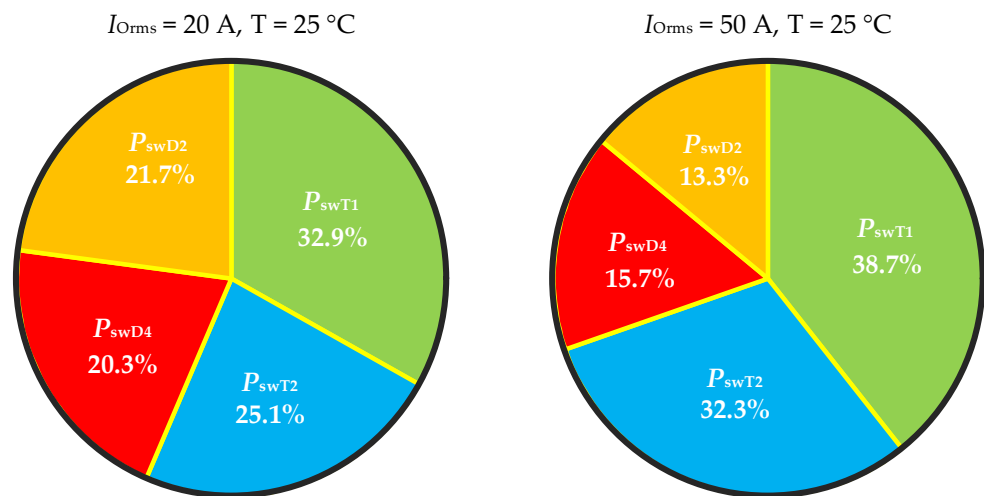


Figure 10. Distribution of switching power losses among TNPC converter devices for phase-shift angle $\varphi = \pi/2$ and rms value of the output current equal to 20 and 50 A.

2.3. DC-Link Capacitor Losses

In addition to power losses in semiconductor devices, this paper also attempts to estimate the losses in both dc-link circuit capacitors C_{dc1} and C_{dc2} , as in Figure 1. Capacitor power losses P_{Cdc} are generated in two capacitors due to non-zero values of equivalent series resistance R_{ESR} and are calculated from Equation (17).

$$P_{Cdc} = 2(I_{dcrms})^2 R_{ESR} = 2(k_{ICdc} I_{Orms})^2 R_{ESR} \quad (17)$$

where I_{dcrms} is the rms value of the capacitor current i_{dc} . The waveform of the capacitor current i_{dc1} is shown in Figure 11.

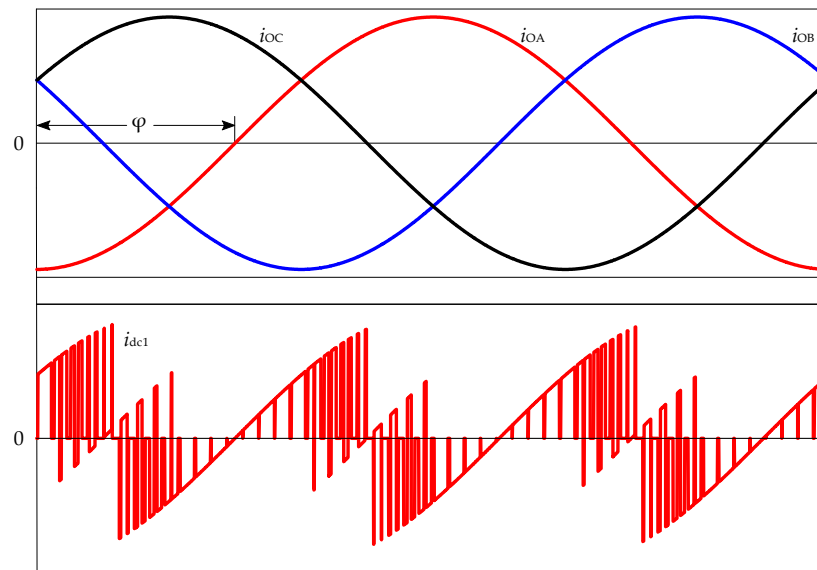


Figure 11. Output currents i_{OA} , i_{OB} and i_{OC} waveforms together with the capacitor current i_{Cdc1} (The switching frequency is intentionally reduced to improve the readability of the capacitor current waveform).

The rms value of the capacitor current depends on phase-shift angle φ , modulation index m_a , the switching frequency f , and output current rms value I_{Orms} . Because the first three listed parameters are set as constant in the paper, it is possible to present the capacitor current rms value only as a function of the output current rms value. The simulation model performed in GeckoCIRCUITS shows that the capacitor current rms value equals 9.75 A when the output current is $I_{Orms} = 20$ A. Because the rms value of the capacitor current depends linearly on the output current, the ratio of these currents is always constant and equals $k_{ICdc} = 9.75 \text{ A}/20 \text{ A} = 0.488$.

In the analysed converter, the equivalent series resistance of capacitor batteries, measured for a frequency of 20 kHz, is equal to $R_{ESR} = 35 \text{ m}\Omega$; thus, total capacitor power losses can be calculated from Equation (17) and given as a function of the output current, as is shown in Figure 12.

It is evident from Figure 12 that the power losses in capacitors account for less than 10% of the conduction losses or switching losses generated in semiconductor devices, and these losses should not be ignored in the power loss analysis of the TNPC converter.

2.4. Total Power Losses

The sum of conduction and switching power losses together with capacitor losses are referred to as total power losses. Because the analysed converter operates as a grid-side converter, the modulation index m_a is nearly constant and equal to $m_a = 0.86$, and its influence on power losses is out of the scope of this paper. The switching frequency, a major parameter significantly impacting switching losses, is also set to $f_S = 20 \text{ kHz}$. Dc-link voltage is $V_{dc} = 740 \text{ V}$, satisfying the requirement for $m_a V_{dc}/2 = U_m$, where U_m

is the magnitude of the phase voltage. The capacitor power losses are present for a set temperature of 25 °C because it is assumed that capacitors are located at a relatively large distance from the IGBT module, which is a significant heat source inside the converter. Total power losses as a function of temperature and current are shown in Figure 13.

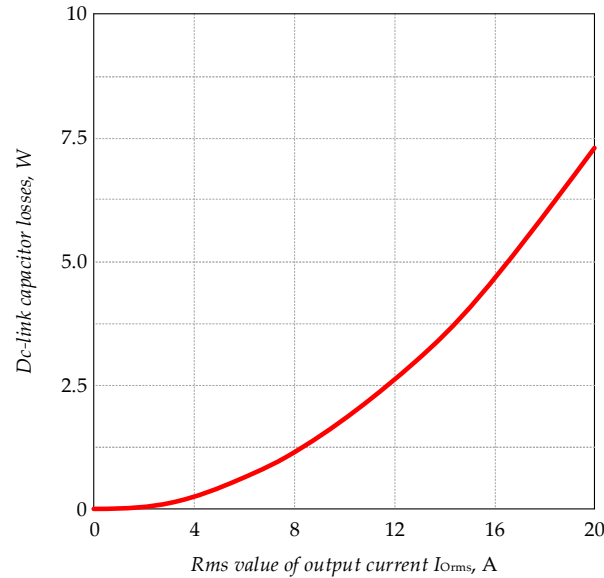


Figure 12. Dc-link capacitor power losses as a function of the rms value of the output current.

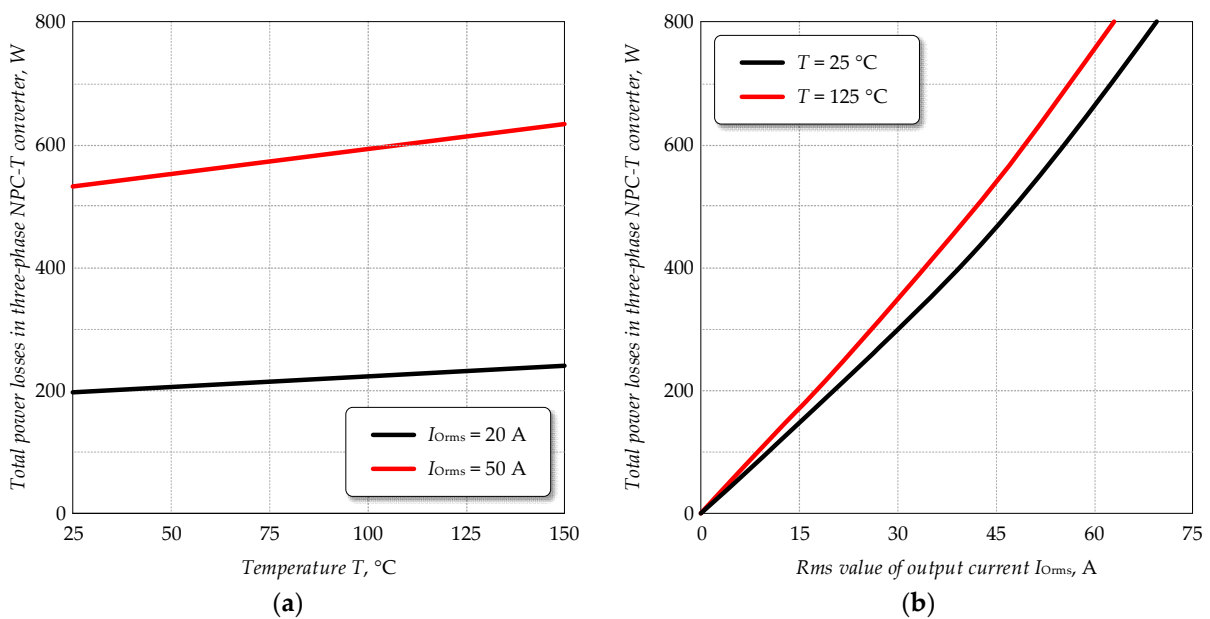


Figure 13. Total power losses in the three-phase TNPC converter are given as (a) a function of temperature T and (b) a function of the rms value of the output phase current I_{Orms} .

The distribution of the sum of power losses ($P_{con} + P_{sw} + P_{Cdc}$) generated in converter components is presented in Figure 14.

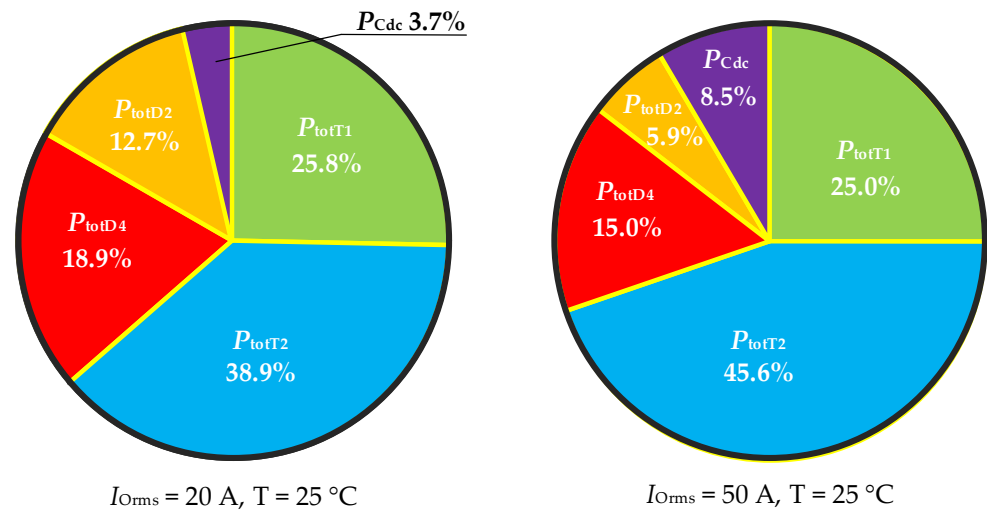


Figure 14. Distribution of power losses generated in TNPC converter devices the output current equal to 20 and 50 A.

2.5. Per kVA Power Loss Ratio

For a converter operating with a large share of reactive power, such as the active power filter, the classical definition of converter efficiency cannot be applied. This is because the converter is connected to one power port, and there are no input and output powers as other converters transfer active power between power ports. In this paper, power losses are referenced to the apparent power as Equation (18), where S_1 is the apparent power for fundamental frequency f_m , and V_{ll} is the line-to-line voltage rms value.

$$R_{loss} = \frac{P_{tot}}{S_1} = \frac{P_{tot}(I_{Orms})}{\sqrt{3}V_{ll}I_{Orms}}, \tag{18}$$

The definition of the power loss ratio is similar to the one used for capacitors used for reactive power compensation. These losses are a function of the output current rms value and are shown in Figure 15. The value of the current equal to 75 A corresponds to the apparent power of 52 kVA.

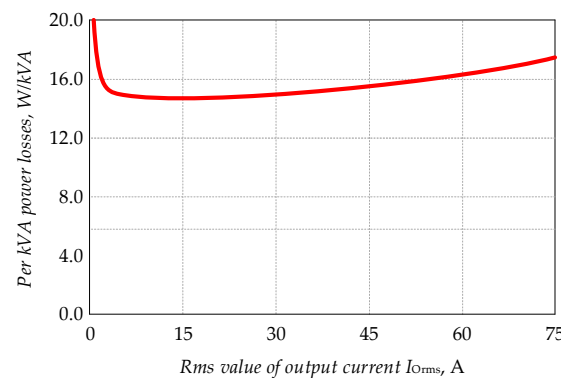


Figure 15. Per kVA power losses of the TNPC converter are given as a function of the output current.

3. Experimental Validation of Power Loss Analysis

The laboratory model of a three-phase TNPC converter has been tested to validate the presented power loss analysis. This laboratory model is a part of a four-wire active power filter with the neutral wire connected to the medium point of the dc-link capacitors [31]. The converter is based on a three-phase TNPC IGBT module 12MBI75VN120-50, the parameters of which are used in the analysis shown in Section 2. For the validation of the power loss analysis, the following two experimental tests have been carried out:

- Test of the TNPC converter supplied from dc power supply operating with a three-phase inductor at the converter output;
- Test of the grid-connected TNPC converter;

Both tests are performed with a nearly constant modulation index $m_a = 0.86$ with a significant reactive component of the output current.

3.1. Power Losses of TNPC Converter Supplied from the DC Power Supply

The converter is supplied from two dc power supplies, each supplying variable voltage $V_{dc}/2$. A three-phase inductor with a nominal inductance of $L_{AC} = 33$ mH is chosen as a load. The sum of the inductor resistance and the resistance of wires equals $R_{LAC} = 0.49 \Omega$ leading to the phase-shift angle $\varphi = 87.6^\circ$. Such a load has been chosen to carry out experimental tests at $V_{dc}/2 = 370$ V with modulation index $m_a = 0.86$, at which the output current rms value equals a rated value $I_{Orms} = I_{On} = 20$ A. The selected value of $V_{dc}/2$ equals the rated value of the tested active power filter. The switching frequency is 20 kHz. The tests have been carried out with a WT5000 power analyser connected to the converter, as shown in Figure 16. The photograph of the experimental setup is presented in Figure 17.

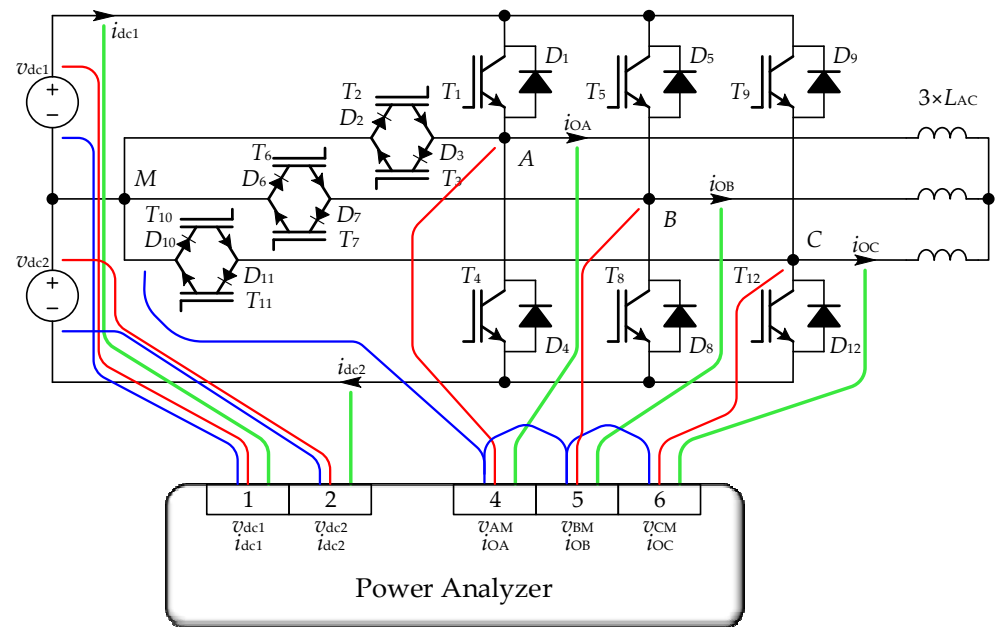


Figure 16. Schematic of the experimental setup for power loss measurement in the three-phase TNPC converter supplied from dc power supplies and with three-phase inductors L_{AC} at the converter output.

The results of power loss measurements are collected in Table 7. During the test, five input elements were used, two for the dc-side of the converter and three for the ac-side. Power is measured at the input as P_{in} and the output as P_{out} , together with calculating the power losses as their difference. Figure 18 shows the exemplary screen images from the power analyser for the rms output current $I_{Orms} = 20$ A.

Table 7. Results of power loss measurement of TNPC converter operating with 33 mH inductors.

v_{dc1}, V	v_{dc2}, V	i_{dc1}, A	i_{dc2}, A	P_{in}, W	I_{Orms}, A	P_O, W	P_{tot}, W
202.90	201.09	0.580	0.638	241.83	11.056	156.69	85.15
254.04	251.52	0.703	0.774	366.96	13.852	245.68	121.28
305.07	302.10	0.827	0.913	518.79	16.649	354.74	164.07
356.04	352.55	0.956	1.056	700.15	19.451	485.50	214.65
370.24	370.59	1.003	1.109	768.90	20.338	534.20	234.70

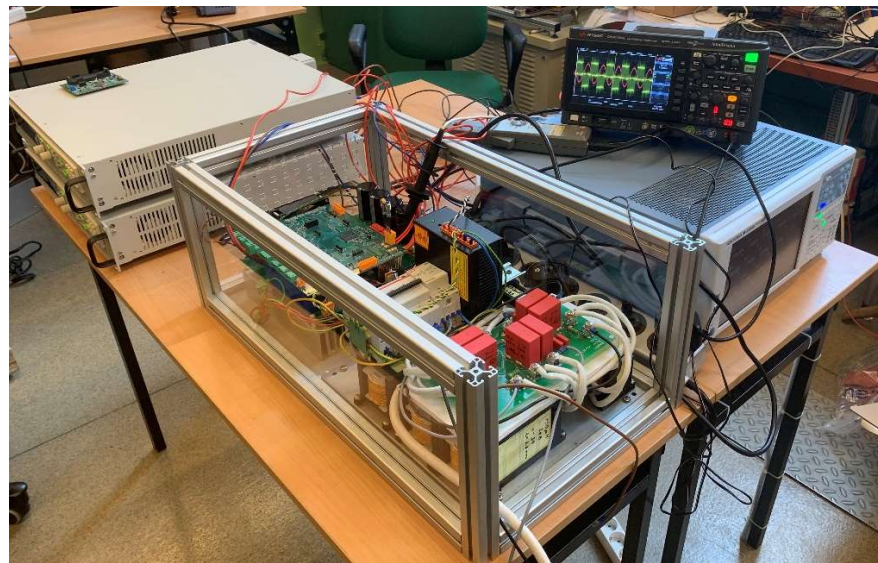


Figure 17. Experimental setup for power loss measurement in the three-phase TNPC converter.

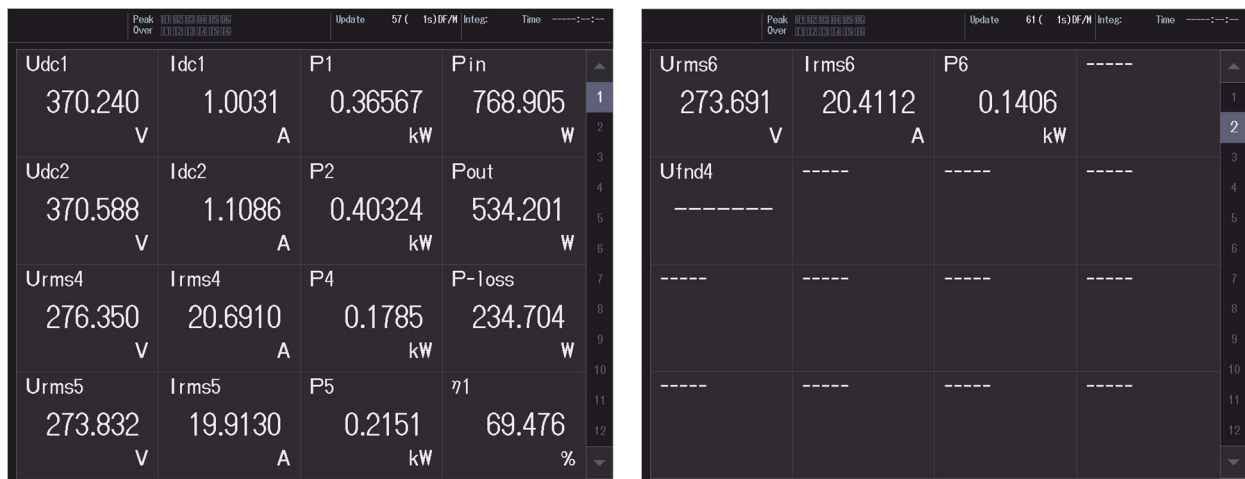


Figure 18. Results for power loss measurement from the WT5000 power analyser.

In Table 7, the measurement data for the dc-side are represented by two voltages, v_{dc1} and v_{dc2} , and currents i_{dc1} and i_{dc2} . For the ac-side, due to the space limitation, only one current I_{Orms} is given, which is the average value of the three-phase currents. The difference between these currents (Figure 18) results from using a three-phase three-limb coupled inductor in which the lowest current occurs in the phase where the winding is wound around the centre limb.

The measured power losses and theoretical total power losses, given for conditions during the test, are shown in Figure 19 as a function of the output current.

The theoretical losses are presented for an assumed temperature $T = 45\text{ }^\circ\text{C}$, the varying blocking voltage, constant phase-shift angle $\varphi = 87.6^\circ$, and modulation index $m_a = 0.86$. The phase-shift angle is adopted from each phase active power measurement according to Equation (19). The reason for the temperature T selection was that a forced cooling system set this temperature as a steady-state thermal value.

$$\varphi = \arctan\left(\frac{\omega L_{AC}}{R_{AC}}\right) = \arctan\left(\frac{\omega L_{AC}}{\frac{1}{3}\left(\frac{P_A}{I_{OArms}^2} + \frac{P_B}{I_{OBrms}^2} + \frac{P_C}{I_{OCrms}^2}\right)}\right), \quad (19)$$

where P_A , P_B and P_C are phase A, B and C output powers and $I_{OA_{rms}}$, $I_{OB_{rms}}$ and $I_{OC_{rms}}$ are corresponding rms values of phase currents. In Equation (19), it was assumed that in each phase, the inductance of the inductor is the same and equal to $L_{AC} = 33$ mH.

From Figure 19, it is evident that the measured losses are higher than the theoretical ones. This is because, in the converter, additional power losses are generated in pcb wires and connectors. The resistance of all wires and connections has been measured and is estimated to be 4.5 m Ω for each converter phase. The characteristic of the theoretical total power losses with additional losses is also shown in Figure 19. The correlation between theoretical and measured losses is high. The presented measurements have been performed for varying dc-link voltage, which did not correspond to the normal operation of the converter. However, they reveal the correct dependence of losses on dc-link voltage.

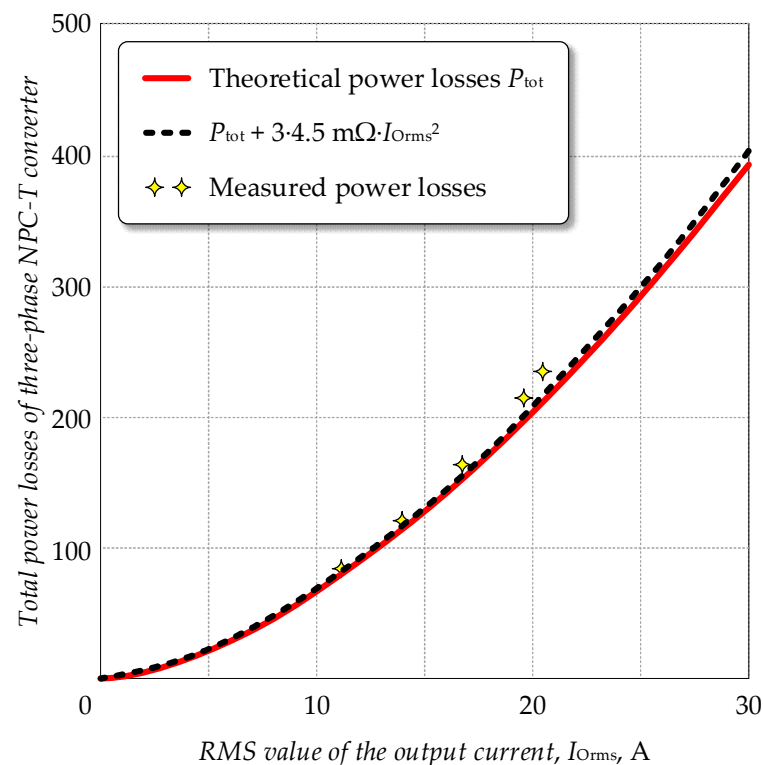


Figure 19. Power losses in the three-phase TNPC converter supplying three-phase inductor $L_{AC} = 33$ mH, operating with a varying dc-link voltage and constant modulation index $m_a = 0.86$.

3.2. Power Losses of Grid-Connected TNPC Converter

In this test, the TNPC converter has been connected to the three-phase 3×400 V grid and operated as the active power filter. The dc-link voltage was kept constant at $V_{dc}/2 = 370$ V. The converter was connected to the grid through the LCL filter with the sum of inductances $L_f = L_{f1} + L_{f2} = 750 + 150 \mu\text{H} = 900 \mu\text{H}$ and filter capacitance $C_f = 4.4 \mu\text{F}$. During the measurement of power losses, the converter has been generating capacitive and inductive reactive power. These power losses are compared with theoretical power losses obtained by applying the method proposed in Section 2. For theoretical power losses, it is assumed that the phase-shift angle $\varphi = 90.0^\circ$ and the modulation index $m_a = 0.86$ for all output current rms values I_{Orms} ranging from $=0$ to 10 A. This assumption also neglects the small capacitive current of the filter capacitor. In the analysis, the switching frequency is considered equal to 20 kHz. The tests have been carried out with a power analyser connected to the converter, as shown in Figure 20.

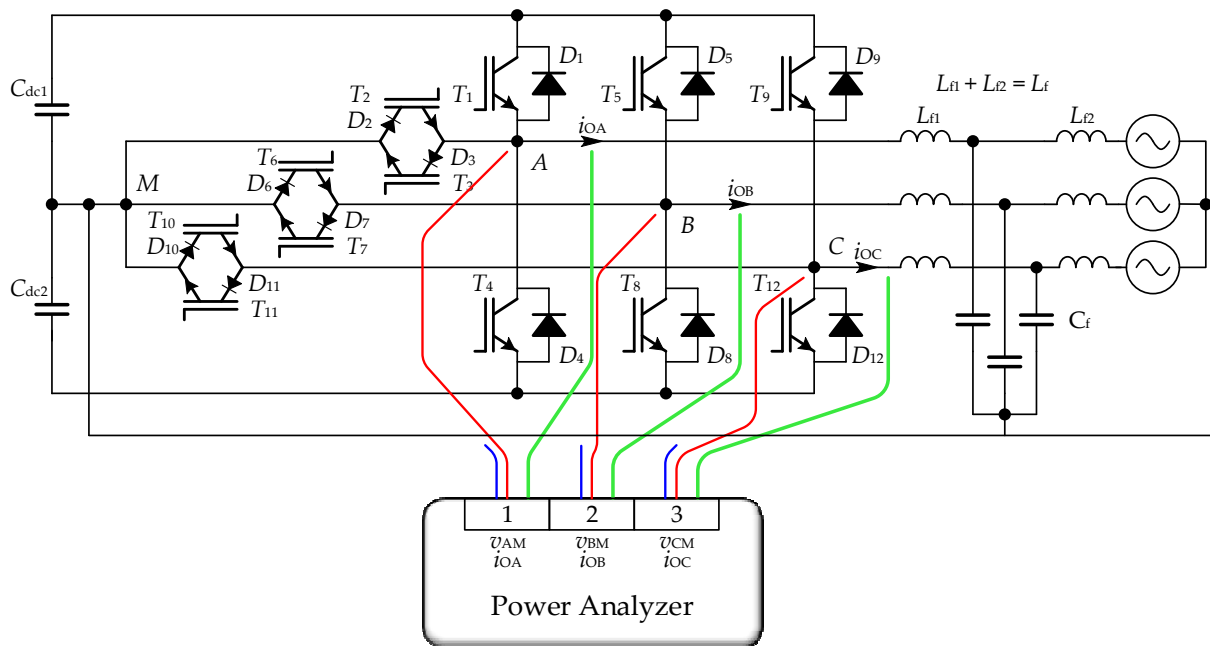


Figure 20. Schematic of the experimental setup for power loss measurement in the three-phase TNPC converter connected to the grid and operating as an active power filter.

The results of the power loss measurements are listed in Table 8, where power losses for inductive output currents are given. The output voltage and current waveforms for inductive reactive power generation at $I_{Orms} = 11.0$ A are shown in Figure 21. The measurement power losses of the three-phase TNPC converter are compared with the theoretical power losses as given in Section 2 and are shown in Figure 22. Apart from generating reactive power, the analysed converter also consumes active power in the form of power losses. Nevertheless, the analysis assumes that the phase-shift angle $\varphi = 90^\circ$. The analysis does not consider the slight change in modulation index m_a with the output current change. Thus, the modulation index is constant and equal to $m_a = 0.86$. Due to a stable thermal condition guaranteed by the cooling system, the temperature during the test was constant and equal to $T = 45$ °C. This temperature was measured by an NTC resistor from the IGBT module.

Table 8. Results of power loss measurement of the TNPC converter operating as the active power filter.

I_{Orms}, A (Inductive)	P_{tot}, W
11.00	120.2
9.90	110.7
8.80	100.4
7.71	90.3
6.61	80.3
5.53	70.2
4.45	60.4
3.40	49.7
2.40	38.7

As seen in Figure 22, the measured power losses are always higher than the theoretical losses. This is particularly true for low rms values of the output current. The main reason for such a difference in power losses is the switching frequency output current ripples. It should be noted that during the first tests, when the converter was supplied from the dc power supply, such output current ripples did not occur due to relatively large inductances of the three-phase inductor, which were equal to $L_{AC} = 33$ mH. Another reason for the discrepancy between measurement data and theoretical results is the assumption that the

device temperature is the same as the temperature of the module base. In a real module, the device temperature is higher by several degrees Celsius.



Figure 21. Exemplary waveforms of the three-phase TNPC converter output voltages and currents for rms value of the output current $I_{Orms} = 11.0$ A and inductive reactive power generation.

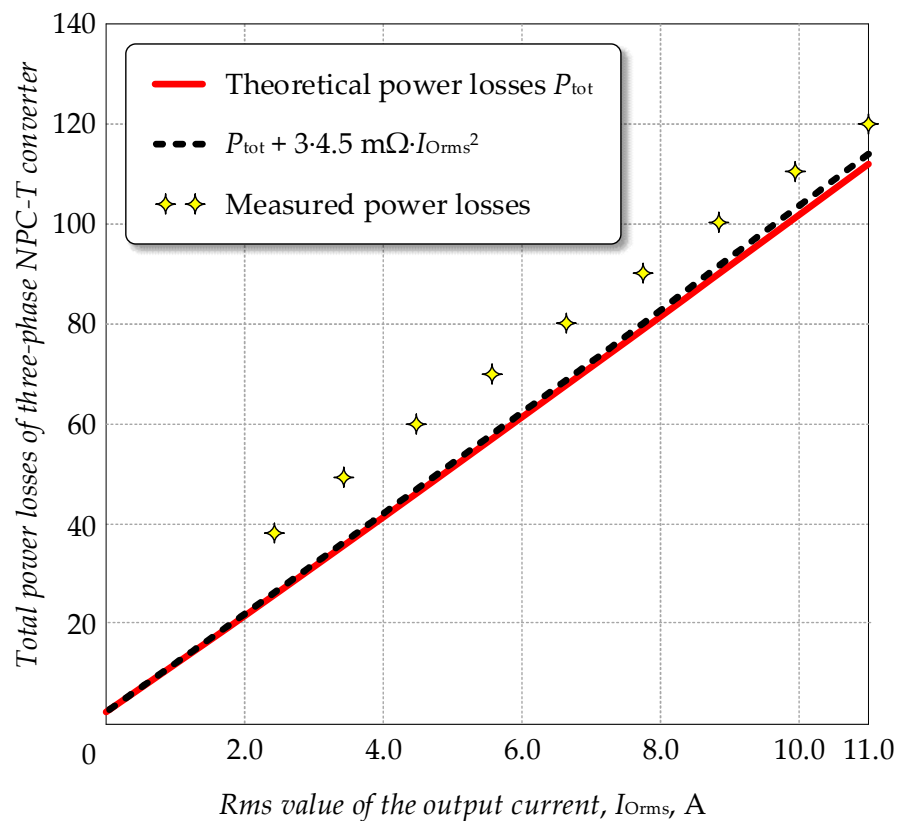


Figure 22. Power losses in the three-phase TNPC converter generating a reactive current.

It should be noted that similar power loss characteristics can be obtained for the generation of capacitive reactive power. In the case of using different design parameters of the active power filter, i.e., with the different switching frequency, dc-link voltage, and temperature, the proposed power loss analysis can also be applied.

4. Conclusions

This paper presents a detailed analysis of power losses of a three-level T-type NPC converter. The study is performed thoroughly; however, the focus is on the converter operation as an active power filter. The accurate recognition of power losses allows the converter designer to carry out the proper steps during the converter designing stages, which, among others, are: setting the switching frequency, designing the cooling system, and designing the gate drivers.

In the paper, the detailed power loss analysis is based on characteristics provided by the IGBT module manufacturer. Obtained power losses are given as functions of the rms value of the output current and temperature. However, they can be extended to other parameters influencing them. Power losses are divided into conduction and switching losses with a given distribution among all semiconductor devices of the T-NPC converter. This division of power losses is essential for designers of IGBT modules and converters because it is possible to find the semiconductor device with the highest power losses for different operating conditions. In the analysed converter operating as the active power filter, the most significant share of losses occurs in transistors T_2 and T_3 . Together with losses in diodes D_2 , they constitute nearly half of the total power losses. These even shares of power losses are a very advantageous feature of the converter.

The measured power losses agree with the losses obtained from the analysis. In the first test, the converter output current has been changed from 10 to 20 A. The difference between the analytical results and measured power losses ranged from 5% to 9%. It is believed that such a good correlation between the measured and analysed results is due to the very small output current ripples in the test, which are neglected in the analysis.

In the second test of the TNPC converter operating as an active power filter, the power losses from the analysis were consistent with the measurements, but better results were obtained for operation at higher currents, close to 11 A. For lower currents, the compliance is lower. This is believed to be due to the presence of current ripples for lower currents power losses that are not the same as for sinusoidal currents.

The TNPC converter has been tested with the rms values of the current ranging from 0 to 20 A when it was supplied from the dc power supply and from 0 to 10 A when it was connected to the grid. For higher currents, the discrepancy between power losses observed during the experiments and theoretical ones can be explained by the existence of higher component junction temperatures than the single temperature measured on the module and the existence of output current ripples.

The future works on presented detailed power loss analysis can be extended with the thermal model of the IGBT module. In such an extended model, the temperatures of individual semiconductor devices are not the same and are higher than the temperature of the module base plate.

It should be noted that the detailed power loss analysis can also be applied to other converter topologies. In such a case, the modification of some parameters is required that relate to different conduction angles, switching angles and modulation functions.

Funding: This publication is supported by the rector's postdoctoral grant, Silesian University of Technology, 05/050/RGH21/1018.

Institutional Review Board Statement: Not applicable.

Data Availability Statement: Experimental data are available upon request.

Acknowledgments: The author would like to thank Jarosław Michalak and Dawid Buła for their support in preparing the laboratory model of the converter for the experimental test.

Conflicts of Interest: The author declares no conflict of interest.

Nomenclature

a_{YX}, b_{YX}, c_{YX}	Parameters of quadratic functions approximating switching energy characteristics of device X for the Y type of loss
$a_{rrX}, b_{rrX}, c_{rrX}, d_{rrX}$	Parameters of cubic functions approximating reverse recovery energy characteristics of diodes
an_X, bn_X	Parameters of linear approximation of exponent of power function approximating the normalised output characteristic of device X
a_{X0}, b_{X0}	Parameters of linear approximation of device X threshold voltage V_{X0}
a_{Xn}, b_{Xn}	Parameters of linear approximation of device X nominal voltage V_{Xn}
E_{onX}	Turn-on switching energy of device X
E_{offX}	Turn-off switching energy of device X
E_{rrX}	Reverse recovery energy in diode X
f_m	Fundamental frequency, $f_m = 50$ Hz
f_S	Switching frequency
I_{dcrms}	Rms value of dc-link capacitor current
I_m	Output current amplitude
I_n	Device nominal current, $I_n = 75$ A
$i_{dc1}(t), i_{dc2}(t)$	Dc-link capacitor currents
$i_O(\omega t)$	Output current in ωt domain, $i_O(\omega t) = I_m \sin(\omega t - \varphi)$
i_{OA}, i_{OB}, i_{OC}	Phase A, B or C output currents
I_{Orms}	Output current rms value
$i_X(t)$	Current of device X
k_{ICdc}	Constant coefficient revealing the relation between the rms values of capacitor current and output current
k_{RGXY}	Constant coefficient representing the effect of the gate resistance on Y type of switching energy losses for device X
L_{AC}	Load inductance in test 1
m_a	Modulation index
n_X	Exponent of a power function approximating normalised output characteristic of device X
P_{Cdc}	Power losses in both dc-link capacitors
P_{con}	Conduction power losses in a three-phase converter
P_{conX}	Conduction power losses in device X
P_{in}, P_O	Input (dc-link) and output (ac side) powers during test 1
P_{sw}	Switching power losses in a three-phase converter
P_{swX}	Switching power losses in device X
P_{totX}	Total power losses in device X
P_{tot}	Total power losses in the three-phase converter
$p_X(t)$	Instantaneous power of device X due to conduction
R_{ESR}	Dc-link capacitor equivalent resistance
R_{LAC}	Resistance of the load inductor and wires during test 1
R_G	Gate resistance in transistor gate driver circuit
R_{loss}	Per kVA power loss ratio
S_1	Converter apparent power for fundamental harmonic
$S_M(\omega t)$	Modulating signal, $S_M(\omega t) = m_a \sin(\omega t)$
$S_X(t)$	Modulation function of device X
t	Time
T	Temperature of converter devices
T_X	Junction temperature of device X
U_m	Amplitude of the fundamental component of output phase voltage
V_b	Blocking voltage during the switching, in TNPC converter $V_b = V_{dc}/2$
V_{CES}	Device maximum blocking voltages, $V_{CES} = 1200$ V (T_1, T_2)
V_{dc}	Dc-link voltage
v_{dc1}, v_{dc2}	Time varying dc-link capacitor voltages

$v_X(t)$	Voltage across device X
V_{X0}	Threshold voltage of device X
$V_{X0,25}, V_{X0,125}$	Threshold voltage of device X at temperatures 25 and 125 °C
V_{Xn}	Nominal voltage of device X at nominal current I_n
$V_{Xn,25}, V_{Xn,125}$	Nominal voltage of device X at temperatures 25 and 125 °C
X	Device symbol, $X = \{T_1, T_2, T_3, T_4, D_1, D_2, D_3, D_4\}$
Y	Switching type symbol, $Y = \{\text{on, off, rr}\}$
$z_{YX}(T)$	General parameters of approximating functions of switching energies used for representing temperature dependence of coefficients
α_1	Angle at which device starts conducting modulated current
α_2	Angle at which device stops conducting modulated current
α_3	Angle at which device starts switching the modulated current
α_4	Angle at which device stops switching the modulated current
ω	Angular frequency, $\omega = 2\pi f_m$

Appendix A Design Parameters of TNPC Converter

The values of the design parameters of the TNPC converter laboratory model are listed in Table A1.

Table A1. Values of design parameters of the TNPC converter laboratory model.

Parameter	Name	Value
V_{ll}	Rated line-to-line voltage rms value	400 V
I_{On}	Rated phase current rms values	10 A, 20 A
V_{dc}	Dc-link rated voltage	740 V
V_{dc1}, V_{dc2}	Dc-link rated voltage across single dc capacitor	370 V
f_m	Fundamental frequency	50 Hz
f_s	Switching frequency	20 kHz
L_{f1}	Converter side filter inductance	0.75 mH
L_{f2}	Grid side filter inductance	0.15 mH
L_f	The sum of filter inductances	0.90 mH
C_f	Filter capacitance	4.4 μ F
C_{dc1}, C_{dc2}	DC-link capacitor capacitance	1.88 mF

References

- Lai, J.-S.; Peng, F.Z. Multilevel converters—A new breed of power converters. *IEEE Trans. Ind. Appl.* **1996**, *32*, 509–517. [\[CrossRef\]](#)
- Rodriguez, J.; Lai, J.-S.; Peng, F.Z. Multilevel inverters: A survey of topologies, controls, and applications. *IEEE Trans. Ind. Electron.* **2002**, *49*, 724–738. [\[CrossRef\]](#)
- Yu, Y.; Konstantinou, G.; Hredzak, B.; Agelidis, V.G. Power Balance of Cascaded H-Bridge Multilevel Converters for Large-Scale Photovoltaic Integration. *IEEE Trans. Power Electron.* **2016**, *31*, 292–303. [\[CrossRef\]](#)
- Akagi, H.; Fujita, H.; Yonetani, S.; Kondo, Y. A 6.6-kV Transformerless STATCOM Based on a Five-Level Diode-Clamped PWM Converter: System Design and Experimentation of a 200-V 10-kVA Laboratory Model. *IEEE Trans. Ind. Appl.* **2008**, *44*, 672–680. [\[CrossRef\]](#)
- Wilson, A.; Bernet, S. Comparative Evaluation of Multilevel Converters with IGBT Modules for Low Voltage Applications. In Proceedings of the 19th European Conference on Power Electronics and Applications (EPE'17 ECCE Europe), Warsaw, Poland, 11–14 September 2017.
- Kersten, A.; Kuder, M.; Thiringer, T. Hybrid Output Voltage Modulation (PWM-FSHE) for a Modular Battery System Based on a Cascaded H-Bridge Inverter for Electric Vehicles Reducing Drivetrain Losses and Current Ripple. *Energies* **2021**, *14*, 1424. [\[CrossRef\]](#)
- Alnamer, S.S.; Mekhilef, S.; Mokhlis, H.; Tan, N.M.L. A Novel Multilevel DC-Link Three-Phase T-Type Inverter. *Energies* **2020**, *13*, 4186. [\[CrossRef\]](#)
- Kaiser, I.; Eckel, H.-G. Comparison of Different Low Voltage Multilevel Converter Topologies for Distributed Power Generation. In Proceedings of the 2020 22nd European Conference on Power Electronics and Applications (EPE'20 ECCE Europe), Lyon, France, 7–11 September 2020.
- Younis, T.; Mattavelli, P.; Toigo, I.; Corradin, M. Three-Phase Modular Multilevel Converter with Optimized Capacitor Sizing for Low-Voltage Applications. *IEEE Trans. Power Electron.* **2021**, *36*, 13930–13943. [\[CrossRef\]](#)

10. Ch, B.; Muduli, U.R.; Behera, R.K. Performance Comparison of Five-Phase Three-Level NPC to Five-Phase Two-Level Voltage Source Inverter. In Proceedings of the IEEE International Conference on Power Electronics, Drives and Energy Systems (PEDES), Chennai, India, 18–21 December 2018. [CrossRef]
11. Hanyang, Y.; Wenxi, Y.; Zhengyu, L.; Bin, C. A Modified Five-Level Hybrid Converter with Large Output Voltage Range and High Efficiency. In Proceedings of the IEEE 8th International Power Electronics and Motion Control Conference (IPEM-ECCE Asia), Hefei, China, 22–26 May 2016; pp. 1217–1221.
12. Fard, M.T.; Abarzadeh, M.; Noghani, K.A.; He, J.; Al-Haddad, K. Si/SiC hybrid 5-level active NPC inverter for electric aircraft propulsion drive applications. *Chin. J. Electr. Eng.* **2020**, *6*, 63–76. [CrossRef]
13. Di Benedetto, M.; Bigarelli, L.; Lidozzi, A.; Solero, L. Efficiency Comparison of 2-Level SiC Inverter and Soft Switching-Snubber SiC Inverter for Electric Motor Drives. *Energies* **2021**, *14*, 1690. [CrossRef]
14. Kim, T.-J.; Kang, D.-W.; Lee, Y.-H.; Hyun, D.-S. The Analysis of Conduction and Switching Losses in Multi-Level Inverter System. In Proceedings of the IEEE 32nd Annual Power Electronics Specialists Conference (IEEE Cat. No.01CH37230), Vancouver, BC, Canada, 17–21 June 2001; IEEE: Vancouver, BC, Canada, 2001; Volume 3, pp. 1363–1368.
15. Nguyen, H.V.; Lee, D.-C. Comparison of Power Losses in Single-Phase to Three-Phase AC/DC/AC PWM Converters. In Proceedings of the 2015 9th International Conference on Power Electronics and ECCE Asia (ICPE-ECCE Asia), Seoul, Korea, 1–5 June 2015; pp. 940–945.
16. Sadigh, A.K.; Dargahi, V.; Corzine, K.A. Analytical Determination of Conduction and Switching Power Losses in Flying-Capacitor-Based Active Neutral-Point-Clamped Multilevel Converter. *IEEE Trans. Power Electron.* **2015**, *31*, 5473–5494. [CrossRef]
17. Bierhoff, M.; Fuchs, F. Semiconductor losses in voltage source and current source IGBT converters based on analytical derivation. In Proceedings of the 2004 IEEE 35th Annual Power Electronics Specialists Conference (IEEE Cat. No.04CH37551), Aachen, Germany, 20–25 June 2004; pp. 2836–2842. [CrossRef]
18. Graovac, D.; Pürschel, M. *IGBT Power Losses Calculation Using the Data-Sheet Parameters*; Infineon Application Note; Infineon Technologies AG: Neubiberg, Germany, 2009; pp. 1–12.
19. Hafezi, H.; Faranda, R. A New Approach for Power Losses Evaluation of IGBT/Diode Module. *Electronics* **2021**, *10*, 280. [CrossRef]
20. Rodriguez, J.; Bernet, S.; Steimer, P.K.; Lizama, I.E. A Survey on Neutral-Point-Clamped Inverters. *IEEE Trans. Ind. Electron.* **2010**, *57*, 2219–2230. [CrossRef]
21. Nabae, A.; Takahashi, I.; Akagi, H. A New Neutral-Point-Clamped PWM Inverter. *IEEE Trans. Ind. Appl.* **1981**, *IA-17*, 518–523. [CrossRef]
22. Pulikanti, S.R.; Dahidah, M.S.A.; Agelidis, V.G. Voltage Balancing Control of Three-Level Active NPC Converter Using SHE-PWM. *IEEE Trans. Power Deliv.* **2011**, *26*, 258–267. [CrossRef]
23. Tauer, M. The Challenges of Using SiC MOSFET-Based Power Modules for Solar Inverters. In Proceedings of the PCIM Europe 2018, International Exhibition and Conference for Power Electronics, Intelligent Motion, Renewable Energy and Energy Management, Nuremberg, Germany, 5–7 June 2018.
24. Zygmanski, M.; Michalak, J.; Biskup, T.; Kolodziej, H. Power loss evaluation for medium voltage drive system based on back-to-back three-level NPC converter integrated with induction machine. In Proceedings of the 18th European Conference on Power Electronics and Applications (EPE'16 ECCE Europe), Karlsruhe, Germany, 5–9 September 2016. [CrossRef]
25. Schweizer, M.; Kolar, J.W. Design and Implementation of a Highly Efficient Three-Level T-Type Converter for Low-Voltage Applications. *IEEE Trans. Power Electron.* **2013**, *28*, 899–907. [CrossRef]
26. Yuan, X. Analytical Averaged Loss Model of a Three-level T-type Converter. In Proceedings of the 7th IET International Conference on Power Electronics, Machines and Drives (PEMD 2014), Manchester, UK, 8–10 April 2014; Institution of Engineering and Technology: Manchester, UK, 2014. [CrossRef]
27. Anthon, A.; Zhang, Z.; Andersen, M.A.E.; Holmes, D.G.; McGrath, B.; Teixeira, C.A. The Benefits of SiC mosfets in a T-Type Inverter for Grid-Tie Applications. *IEEE Trans. Power Electron.* **2017**, *32*, 2808–2821. [CrossRef]
28. Gurbinar, E.; Castellazzi, A. Single-Phase T-Type Inverter Performance Benchmark Using Si IGBTs, SiC MOSFETs and GaN HEMTs. *IEEE Trans. Power Electron.* **2015**, *31*, 7148–7160. [CrossRef]
29. Kumari, K.; Mapa, S.; Maheshwari, R. Loss Analysis of NPC and T-Type Three-Level Converter for Si, SiC, and GaN based Devices. In Proceedings of the 2020 IEEE 9th Power India International Conference (PIICON), Sonapat, India, 28 February–1 March 2020. [CrossRef]
30. Stefanik, J.; Zygmanski, M. Power Loss Analysis of Advanced-Neutral-Point-Clamped Converter with SiC MOSFETs and Si IGBTs. In Proceedings of the 19th International Power Electronics and Motion Control Conference (PEMC), Gliwice, Poland, 25 April 2021; pp. 161–166.
31. Buła, D.; Jarek, G.; Michalak, J.; Zygmanski, M. Control Method of Four Wire Active Power Filter Based on Three-Phase Neutral Point Clamped T-Type Converter. *Energies* **2021**, *14*, 8427. [CrossRef]
32. Datasheet of TNPC IGBT Module 12MBI75VN120-50. Available online: <https://felib.fujielectric.co.jp/download/details.htm?dataid=5401476&site=global&lang=en> (accessed on 5 July 2022).